Revista Internacional de Investigación e Innovación Tecnológica

Página principal: www.riiit.com.mx

GTAW Butt Welded 6061-T6 Aluminum: Post-process Heat Treatment Effect on Mechanical and Microstructural Features

Aluminio 6061-T6 soldado a tope mediante GTAW: Efecto del Tratamiento Térmico Posterior al Proceso sobre las Características Mecánicas y Microestructurales

Salgado-López, J.M.[a], Cruz-González, C.E.[a], Tello-Rico, M.[a], León-Méndez, I.[a], Guzmán-Flores, I.[b], Granda-Gutiérrez, E.E.[c]*

[a] Dirección de Ingeniería de Manufactura, Centro de Ingeniería y Desarrollo Industrial; C.P. 76125, Santiago de Querétaro, Querétaro.

[b] Facultad de Sistemas, Universidad Autónoma de Coahuila; C.P. 25350, Arteaga, Coahuila.

[c] Centro Universitario UAEM Atlacomulco, Universidad Autónoma del Estado de México; C.P. 50000, Toluca, Estado de México.

msalgado@cidesi.edu.mx; ecruz@cidesi.edu.mx; soldadura@cidesi.edu.mx; ivan.leon@cidesi.edu.mx; isidroguzman@uadec.edu.mx; eegrandag@uaemex.mx*

Technological innovation: In the field of welding of aluminum alloys, focusing on the exhaustive analysis of the mechanical and microstructural properties of the welded joints of 6061-T6 aluminum using the (GTAW) process, affected by temperature and different subsequent thermal treatments to welding.

Industrial application area: Mechanical and metallurgical industry.

Received: november 27th, 2023
Accepted: april 02th, 2024

Resumen

La soldadura de aluminio sigue siendo un área importante de investigación, impulsada por desafíos actuales, como la reducción observada en las propiedades mecánicas después del proceso de unión, comúnmente conocida como ablandamiento. En particular, existe información limitada sobre el impacto de los tratamientos térmicos en las propiedades mecánicas de las uniones en la aleación AA6061. Este estudio aborda esta brecha presentando las propiedades mecánicas en las uniones de esta aleación en tres condiciones distintas: una en su estado soldado y dos sometidas a diferentes tratamientos térmicos posteriores. Los hallazgos revelan que los parámetros del proceso de unión, los defectos, y el tratamiento térmico aplicado influyen en la eficiencia de las juntas. Principalmente, los tratamientos térmicos posteriores ejercen un impacto sustancial en la

microestructura y las propiedades mecánicas finales de la soldadura. El tratamiento de solubilizado disuelve eficazmente los precipitados en la microestructura, mientras que el tratamiento de envejecimiento restaura con éxito las propiedades mecánicas, debido al endurecimiento por precipitación. Sin embargo, es crucial tener en cuenta que los defectos en la unión juegan un papel fundamental en la determinación de las propiedades mecánicas finales y la ubicación de las grietas después de la fractura. Adicionalmente, se estudia la resistencia mecánica de la unión en pruebas de tensión a temperaturas distintas, encontrándose que este parámetro alcanza su punto máximo a bajas temperaturas y disminuye al aumentar la temperatura. Por el contrario, el alargamiento es más significativo a temperaturas elevadas pero reducido a temperaturas más bajas. Este análisis integral aborda la interacción entre las condiciones de soldadura, los tratamientos térmicos y los cambios microestructurales, proporcionando información valiosa para mejorar el proceso de unión e incrementar el rendimiento mecánico en juntas de aluminio AA6061-T6.
Palabras clave: Aleaciones de aluminio, Soldadura, Tratamiento térmico, Propiedades mecánicas, Microestructura.

Abstract

Welding of aluminum remains an important area of research, driven by current challenges**,** such as the observed reduction in mechanical properties after the joining process, commonly referred to as softening. Particularly, there is limited information on the impact of heat treatments on the mechanical properties of joints in AA6061 alloy. This study addresses this gap by presenting mechanical properties of AA6061 joints under three distinct conditions: one in its welded state and two subjected to different subsequent heat treatments. Findings reveal that joining process parameters, defects, and applied heat treatment influence joint efficiency. Primarily, subsequent heat treatments substantially impact the microstructure and final mechanical properties of the weld. Solubilizing heat treatment effectively dissolves precipitates in the microstructure, while aging treatment successfully restores mechanical properties due to precipitation hardening. However, it is crucial to note that joint defects play a key role in determining final mechanical properties and crack location post-fracture. Additionally, the mechanical strength of the joint is studied in tensile tests at different temperatures, finding that this parameter reaches its maximum value at low temperatures and decreases with increasing temperature. In contrast, elongation is more significant at higher temperatures**,** but reduced at lower temperatures. This comprehensive analysis addresses the interaction between welding conditions, heat treatments, and microstructural changes, providing valuable information for improving the joining process and enhancing mechanical performance in AA6061-T6 aluminum joints.
Keywords: Aluminum alloys, Welding, Heat treatment, Mechanical properties, Microstructure.

1. Introduction

The use of aluminum alloys in structural applications has significantly increased in recent years due to their advantageous properties[1,2]. Welding emerges as the primary joining process for such materials, with Gas Metal Arc Welding (GMAW) and Tungsten Metal Arc Welding (GTAW) widely employed in the industry. Consequently, the

guidelines for aluminum structural welding are outlined in the AWS D1.2 welding code[3].

However, welding aluminum alloys is challenging, primarily because of the high reactivity of aluminum. Overcoming issues such as porosity, cracking, shrinkages, softening, and the formation of a large heat-affected zone (HAZ) poses difficulties, a problem encountered in both conventional processes (GTAW and GMAW) and newer techniques like laser beam welding and cold metal transfer. Post-welding heat treatments present a viable avenue for mitigating the impact of these defects, making them a focal point of current research.

Numerous researchers have studied the relationship between aluminum welding processes and the resulting mechanical properties[4]. For instance, Ramaswamy et al.[5] explored the effects of post-weld heat treatment on the tensile properties of cold metal arc welded AA 6061-T6 aluminum joints, revealing a 10% increase in tensile strength after treatment. Rathinasuriyan et al.[6] compared the mechanical and metallurgical properties of GTAW, GMAW, and FSW (Friction Stir Welding) lap joints on AA6061-T6 alloy, establishing correlations between properties and welding parameters. Guzman et al.[7] examined the tensile and fracture behavior in 6061-T6 and 6061-T4 aluminum alloys welded by pulsed metal transfer GMAW, highlighting the impact of welding defects on the final mechanical properties.

In addition, Rodriguez-Hernandez et al.[8] investigated the microstructure and mechanical properties of GTAW-GMAW hybrid welding of AA 6061-T6 Aluminum alloy, noting a reduction in final mechanical strength after artificial aging. Soundararajan et al.[9] explored the enhancement of tensile strength in AA 6061-T6 plates joined by gas tungsten arc welding using a high entropy alloy filler metal.

In the case of 6061 aluminum alloys, the softening of the base material during the welding process is the most common reason for failing to achieve the minimum tensile properties requirement of a weld made with this base material without significant discontinuities. For instance, the 6061-T6 base material has a typical tensile strength of 310 MPa before welding, but the AWS D1.2 requires a minimum tensile strength of 165 MPa[3]. If inappropriate parameters are used during the joining process, the excessive softening of the weld could reduce the tensile strength below the required minimum.

The softening after aluminum welding is caused by the welding heat input, which results in metallurgical changes in the base material. Thus, to reach the minimum tensile strength requirements of the code, the welding procedure must be closely controlled to prevent overheating of the base material or to apply a post-welding heat treatment that restores the mechanical properties[10].

Despite the extensive literature on aluminum welding, there is a lack of information on AA6061 weldments subjected to different post-welding heat treatments and their effect on tensile strength. This is particularly relevant considering the prevalent use of single-pass butt joints in aluminum welding applications. Consequently, this study aims to comprehensively analyze the mechanical properties, fracture surfaces, microhardness profiles, and microstructure of AA 6061-T6 welded joints, with and without one of two post-welding heat treatments applied: a cryogenic treatment and a weld followed by aging. The findings could improve the applications of this type of aluminum alloy.

2. Experimental methods

2.1.Manufacturing of test samples

To achieve the objectives of this study, welding test coupons were fabricated using 6061-T6 aluminum alloy, measuring 30 mm x 30 mm in length and width, respectively, and 6 mm in thickness, as illustrated in Figure 1.

Manual GTAW equipment was employed to weld the test coupons, utilizing a 3mm 5053 filler metal and a 3-mm diameter EWLa-1.5 electrode. Process conditions included a welding current of 250 A, voltage of 15 V, and preheating at 160 °C for both the initial and subsequent welding. The welding parameters were in accordance with the specifications in the AWS D1.2 code and guidelines for filler metals. Due to the manual welding of AA6061-T6 coupons, precise measurement of welding speed was not possible. As an approximation, utilizing the AWS equation for heat input[2,3] and assuming a travel speed of 25 mm/min, the calculated heat input was 9 kJ/mm. However, considering the thermal efficiency of 0.6 for GTAW, the adjusted heat input was 5.4 kJ/mm.

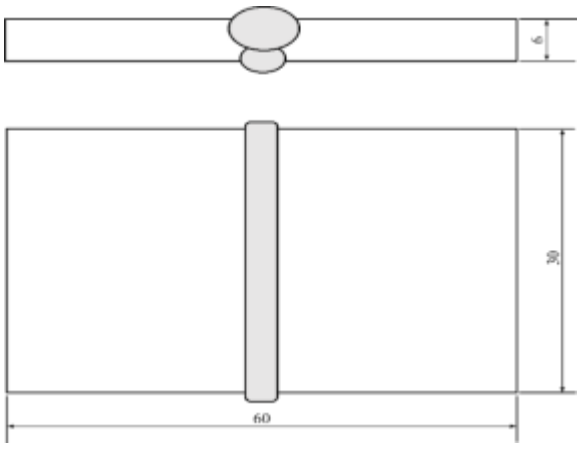

Figure 1. Test coupons for the welding process.

Three distinct conditions were selected to assess the mechanical properties of the welded joints, which were labeled as follows:

1. AW for weld coupons without subsequent heat treatment.
2. CR for weld samples with a cryogenic treatment. The CR treatment involved heating the welded coupons to 180 °C in an atmospheric furnace for 12 hours, followed by air cooling and immersion in a liquid nitrogen bath at -185 °C for 15 minutes.
3. HT for welded coupons with a dissolution heat treatment followed by aging. The HT treatment comprised a dissolution at 530 °C for 1 hour in a vacuum furnace at a pressure of 10^{-3} MPa, followed by quenching in nitrogen gas at 0.5 MPa (5 bar) in the furnace. Subsequently, the test coupon was reheated to 180 °C for 6 hours and then cooled in nitrogen inside the furnace.

2.2 Mechanical testing

To determine the mechanical properties of each metallurgical condition (AW, CR, and HT) and to calculate joint performance, ASTM E8[11] compliant undersized test specimens were precision-manufactured using a VF2 HASS® machine. Subsequently, these specimens underwent testing using an INSTRON® 100 kN AGX-V universal testing machine equipped with knurled grips.

The tensile strength tests were conducted at different temperatures. They were set at -20 °C for low-temperature specimens (designated as “Lt”), 25 °C for room temperature specimens (referred to as “Rt”), and 90 °C for high-temperature samples (referred to as “Ht”). The Lt and Ht specimens were conditioned in the TCE-N300 chamber for 30 minutes at their respective temperatures. In contrast, the Rt specimens were directly mounted between machine grips for testing.

To determine tensile properties, the testing protocol involved a speed of 5 MPa/min (for yield) and 5 mm/min. The yield strength at 0.2% and stress-strain diagrams were derived

using a 25 mm length ST Epsilon clip extensometer. The resulting mechanical properties of the Rt, Lt, and Ht samples subjected to post-welding heat treatments were systematically compared against the mechanical properties of the AW specimens.

The microhardness profile illustrates the distribution of hardness across the weldment. For this study, the microhardness profile of each condition was determined using a TUKON 1202 microhardness tester, employing a 100 g load for a dwell time of 10 seconds. This testing methodology allows for precise hardness measurements at various points within the weld, providing valuable data on the material's hardness characteristics and potential variations across different metallurgical conditions.

2.3 Metallographic and SEM evaluation

For metallography, a representative sample from each condition was extracted by a cross-section of the welded joint in one specimen per condition. The test specimens, measuring 2mm×1mm×6mm, were prepared according to ASTM E3[12]. Subsequently, the specimens underwent sequential grinding using 320 to 1200-grit sandpaper and polishing with 1-micron diamond paste. The microstructure of the test samples was then etched using Keller's reagent.

Macrostructures were observed using a Leica stereographic microscope, while microstructures were examined using a Nikon Epihot 440 microscope, complemented by image analysis software. Elemental chemical microanalysis was conducted using a scanning electron microscope, specifically the JEOL JSM 6610LV (SEM), coupled with an Energy Dispersive Spectroscopy (EDS) microanalysis probe. This comprehensive approach allowed for a thorough examination of the macro and microstructural features of the weldments, providing a valuable understanding of their composition and characteristics.

The fracture surface of representative test samples from each tensile-tested condition (AW, CR, and HT) was examined using a JEOL JSM-6610LV scanning electron microscope (SEM). The SEM images were captured at 350X magnification, utilizing secondary electrons, with an operating voltage of 15 kV and a working distance of 10 mm. This analytical approach provides detailed insight into the morphology and characteristics of the fracture surfaces under different metallurgical conditions, aiding in the comprehensive understanding of the material's behavior under tensile loading.

3. Results

3.1. Mechanical properties at -20 ºC, 25 ºC and 90 ºC

The results of the tensile tests conducted at different temperatures are presented in Table 1. Analysis of the as-welded (AW) samples indicated a negligible variability in tensile strength between room temperature (Rt) and high temperature (Ht), with a slight reduction in yield strength observed for low temperature (Lt) conditions. In contrast, the cryogenically treated (CR) sample results exhibited the highest tensile strength at -20 °C, surpassing the Rt specimens by 8 MPa, and the lowest tensile strength at 90 °C, showing a 9 MPa decrease compared to Rt specimens. A similar trend in yield strength of 0.2% yield stress was observed for CR samples.

The results from the heat-treated (HT) specimens showed a minimal variation in the tensile strength values at 25 °C, with a slight decrease of 3 MPa at 90 °C. However, the yield strength exhibited the lowest variation (1 MPa) at -20 and 90 °C, with the weakest strength observed at 25 °C. AW specimens

and most of the CR test specimens experienced fractures within the heat-affected zone (HAZ), whereas HT specimens fractured within the weld metal. Additionally, all three sets of test specimens exhibited substantial plastic deformation indicative of a ductile fracture[13].

Table 1 illustrates the differences in elongation among the three sets of test specimens (AW, CR, and HT). The elongation is most significant for all specimens at Ht. However, the difference in elongation at Lt or Rt is minimal, influenced by welding defects that impacted the overall mechanical behavior of the samples.

Tensile testing of the base metal at 25 °C for the 6061-T6 alloy exhibited a tensile strength of 322 MPa, a 0.2% yield stress of 277 MPa, an elastic modulus of 67 GPa, and an elongation of 22%. Conversely, testing at high temperatures (Ht, 90 °C) revealed a tensile strength of 298 MPa, a 0.2% yield stress of 274 MPa, and an elongation of 32%. At low temperatures (Lt, -20 °C), the base metal specimens displayed a tensile strength of 320 MPa, a 0.2% yield stress of 283 MPa, and an elongation of 23%. These results are in line with the data reported in technical literature[14].

Table 1. Average test results for ultimate tensile strength, elongation yield stress, and elastic modulus.

Heat treatment	*Testing temperature (°C)*	*Ultimate Tensile strength (MPa)*	*0.2% yield stress (MPa)*	*Elastic modulus (GPa)*	*Elongation (%)*	*Fracture location/weld defect detected by the naked eye*
AW	*-20*	*165±1.0*	*85±5.9*	*68±2.7*	*9.71±2.72*	*HAZ/ one in weld metal with lack of fusion*
	25	*165±0.5*	*92±0.5*	*66±4.7*	*13.1±*	*HAZ / not defect detected*
	90	*166±0.5*	*93±1.5*	*61±0.2*	*15.12±2.2*	*HAZ/ not defect detected*
CR	*-20*	*170±0.1*	*117±7.9*	*67±0.9*	*4.45±1.83*	*HAZ/ not defect detected*
	25	*162±0.5*	*112±15.4*	*61±5.9*	*4.39±2.6*	*HAZ/ not defect detected*
	90	*153±1.5*	*106±14.0*	*63±0.2*	*13.65±0.5*	*Weld metal and HAZ / lack of fusion on weld metal of one specimen*
HT	*-20*	*247±0.5*	*134±6.0*	*65±0.3*	*7.65±0.5*	*Weld metal/pores*
	25	*247±9.0*	*129±5.2*	*61±0.7*	*9.36±5.3*	*Weld metal/pores*
	90	*244±0.7*	*133±14.0*	*63±0.7*	*27.5±5.1*	*Weld metal/ pores*

The joint efficiency for the as-welded (AW) test specimens was determined to be 51% of the base metal tensile strength. In the case of cryogenically treated (CR) samples, a joint efficiency of 53% was observed at -20 °C, while 50% was measured at room temperature (Rt) and 47% at high temperature (Ht). Notably, for heat-treated (HT) test samples, there was a significant increase in joint efficiency, reaching 76%. It is essential to highlight that, except for the CR sample at 25 °C, all test specimens met the specifications outlined in the AWS D1.2[3] welding code for aluminum alloys.

Figure 2 illustrates the profiles of micro-Vickers hardness, showing distinct trends among the as-welded (AW), cryogenically treated (CR), and heat-treated (HT) samples. AW and CR samples' micro-Vickers hardness profiles exhibit similarities but diverge notably in the base metal. Sample AW present an average of 55 HV on the base metal, while sample CR exhibits an average of 66 HV in

the same zone. Conversely, the HT sample demonstrates the highest hardness values, reaching approximately 115 HV on the heat-affected zone (HAZ) and 100 HV on the base metal.

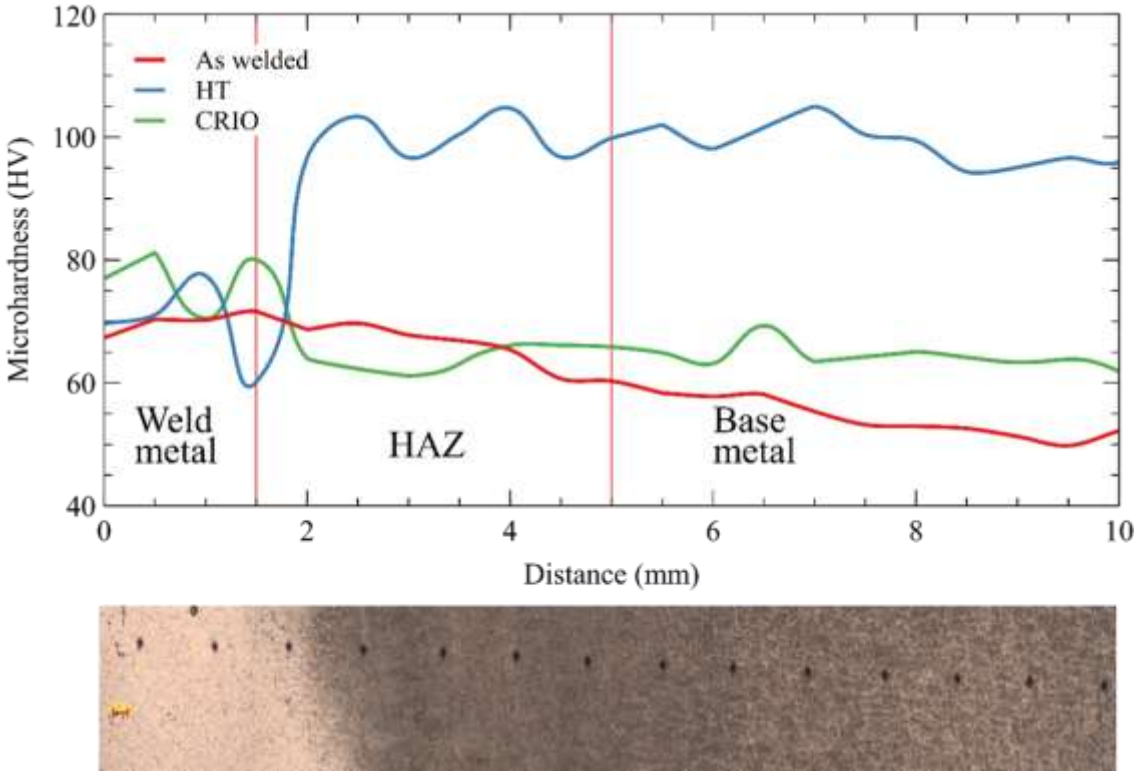

Figure 2. Microhardness profile of the tested samples (100X magnification).

It is important to note that both HT and CR samples exhibit scattered hardness values, whereas the base metal follows a smoother trend. Remarkably, the HAZ boasts Vickers Hardness values around 115 HV for the HT sample, representing a notable 12% increase compared to the base metal of the same sample. This observation emphasizes the impact of different treatments on the microhardness distribution, indicating the variations in material properties across the weld. The variations in microhardness are attributed to microstructural changes. In welding, there is a dendritic solidification structure characterized by lower hardness, while in the diffusion-affected zone, there is grain fracture or breakage. Additionally, as one progresses from the diffusion zone to the base metal, although not explicitly investigated in this study, there is always a grain size transformation. In both the diffusion zone and the heat-affected zone, there is phase dissolution and precipitation of other phases, such as the β phase, also known as the hardening phase, characteristic of this type of alloy.

3.2.Macrostructure and Microstructure Analysis

As a reference, the macrostructure examination of the base metal (prior welding) revealed a banded material with no detectable evidence of defects, as depicted in Figure 3.

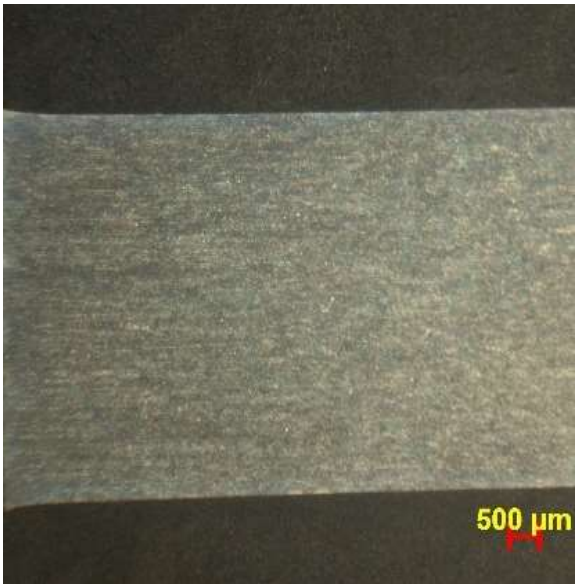

Figure 3. Macrograph of the base metal at 10X.

Figures 4a-c offer a detailed examination of the macrostructure at 20X magnification under each test condition (AW, CR, and HT) after welding and the subsequent heat treatment (see section 2.1). The macrographs show the presence of minor pores within the weld metal. However, no indications of cracking in the Heat Affected Zone or other defects near the weld zone (such as incomplete fusion, excessive porosity, or cavities), nor in the metal base (such as cracks, overheating, or excessive penetration), were observed.

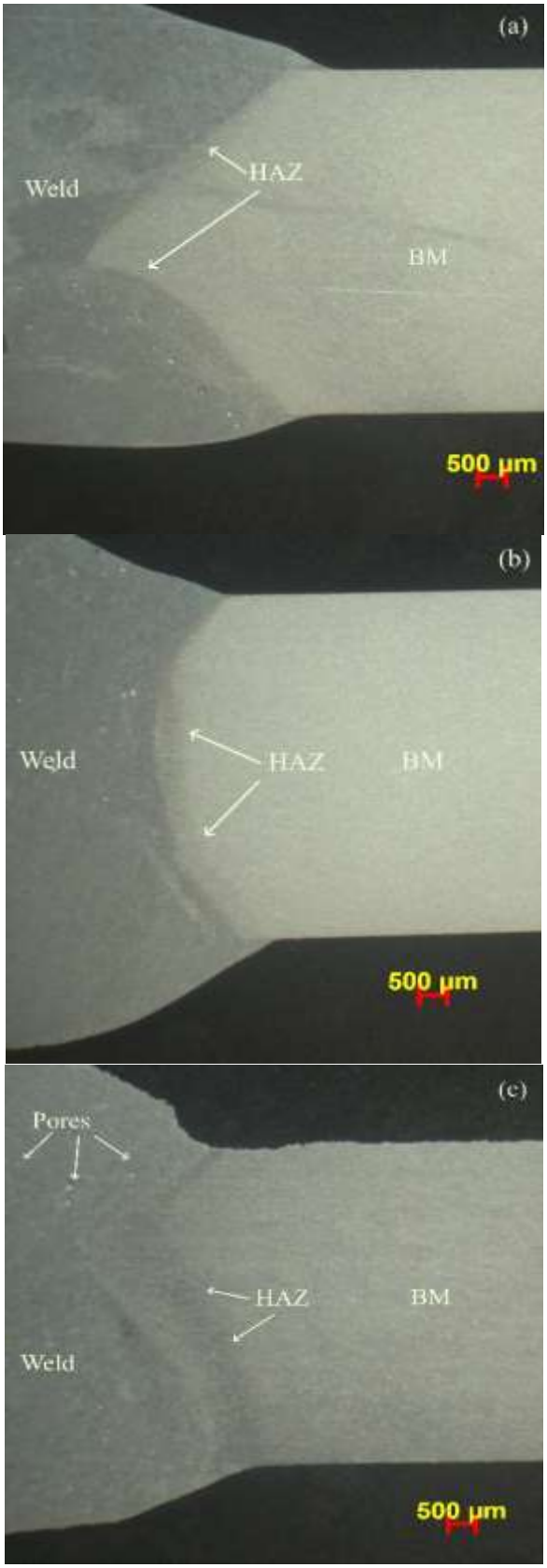

Figure 4. Macrographs at 20X magnification for the AW (a), CR (b), and HT(c) conditions.

In Figure 5, the microstructure of the base metal at 200x is presented, revealing fine phases within the grains and coarser phases along the grain boundaries. This microstructure matches with the well-documented microstructure of AA6061-T6[1,2].

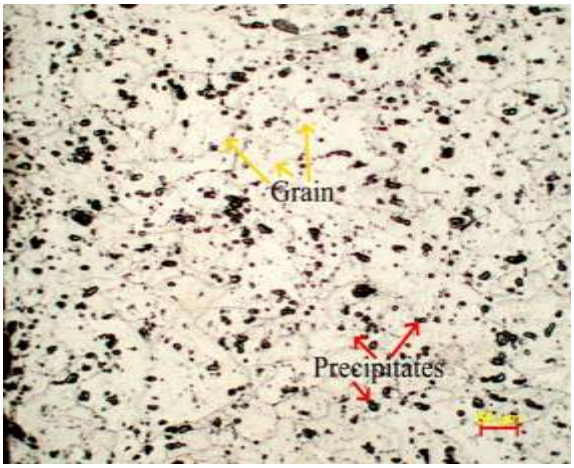

Figure 5. Microstructure at 200X of the base metal, showing Mg2Si precipitates (red arrows) and fine elongated grains (yellow arrows).

Figure 6, illustrates the 200X microstructure of the welded joint in the as-welded (AW) condition. Dendrites are observed in the weld metal, along with coarse precipitates in the HAZ and elongated fine grains with precipitates in the base metal. As reported in the literature, the precipitates of Mg_2Si and FeSiAl in the HAZ of AA6061 were confirmed through EDS microanalysis, in line with existing information[5–7].

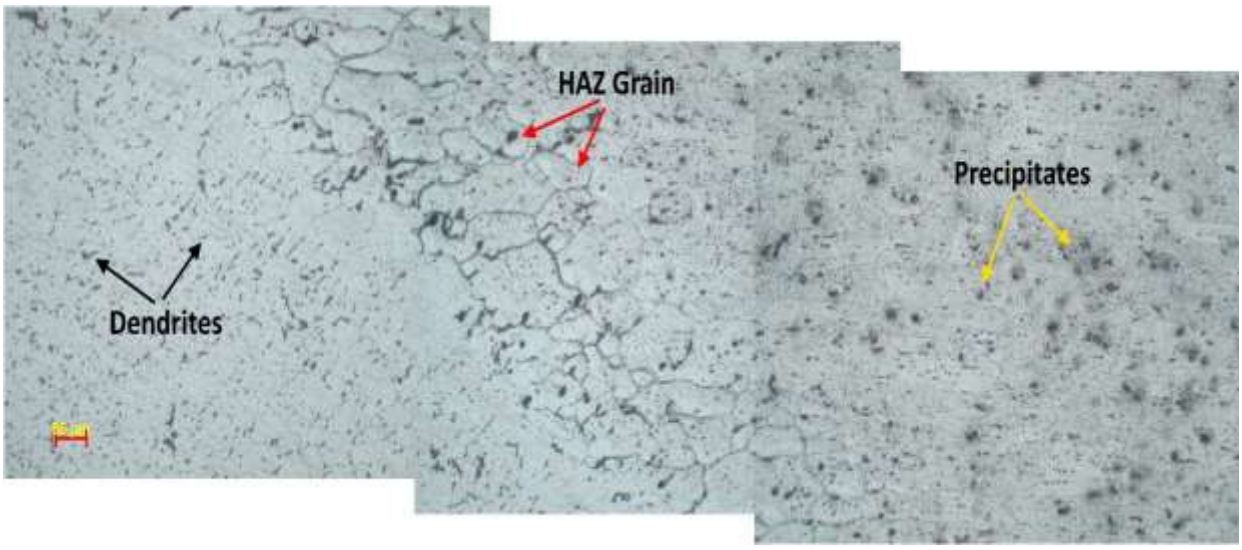

Figure 6. Microstructure at 200x of the AW sample. This is a mapping of the weld region showing Dendrites (black arrows) in the weld zone, elongated grains (red arrows) in the HAZ, and coarse precipitates (yellow arrows) in the base metal near the HAZ.

Figure 7 shows the microstructure at 200X of the weld joint in the cryogenically treated (CR) condition, with dendrites in the weld metal and coarse precipitates in the HAZ and base metal. Similarly, Figure 8 exhibits the microstructure at 200X of the weld joint in the heat-treated (HT) condition, with dendrites in the weld metal and fine precipitates in the HAZ and base metal.

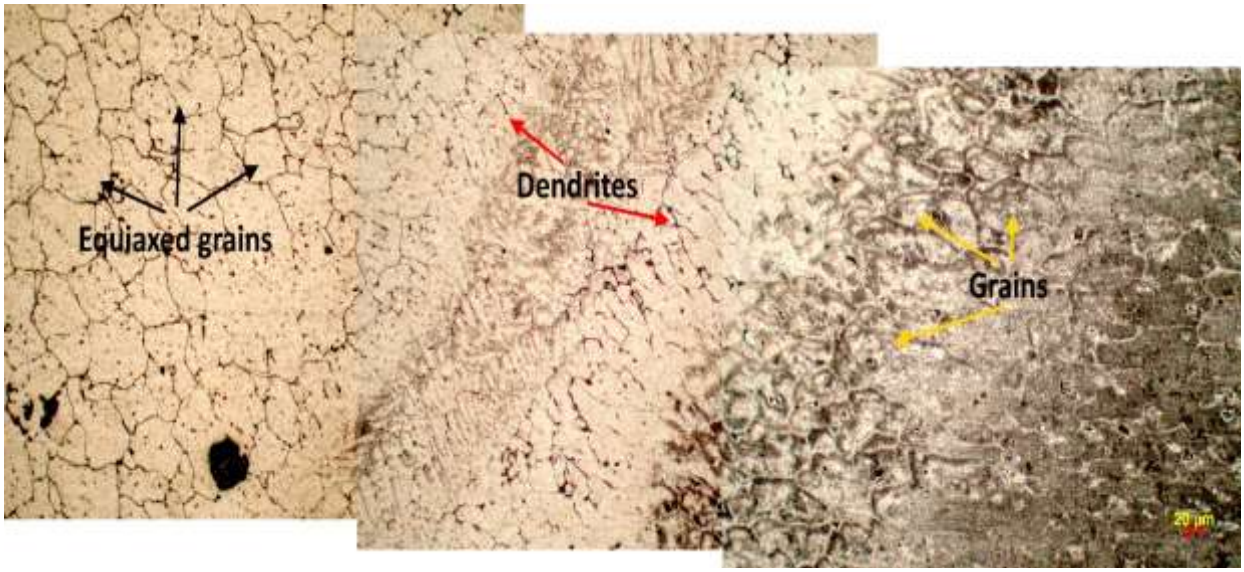

Figure 7. Microstructure at 200X of the CR sample. The micrograph shows elongated equiaxed grains (black arrows) in the HAZ, Dendrites (red arrows) in the weld metal, and grains in the base metal (yellow arrows).

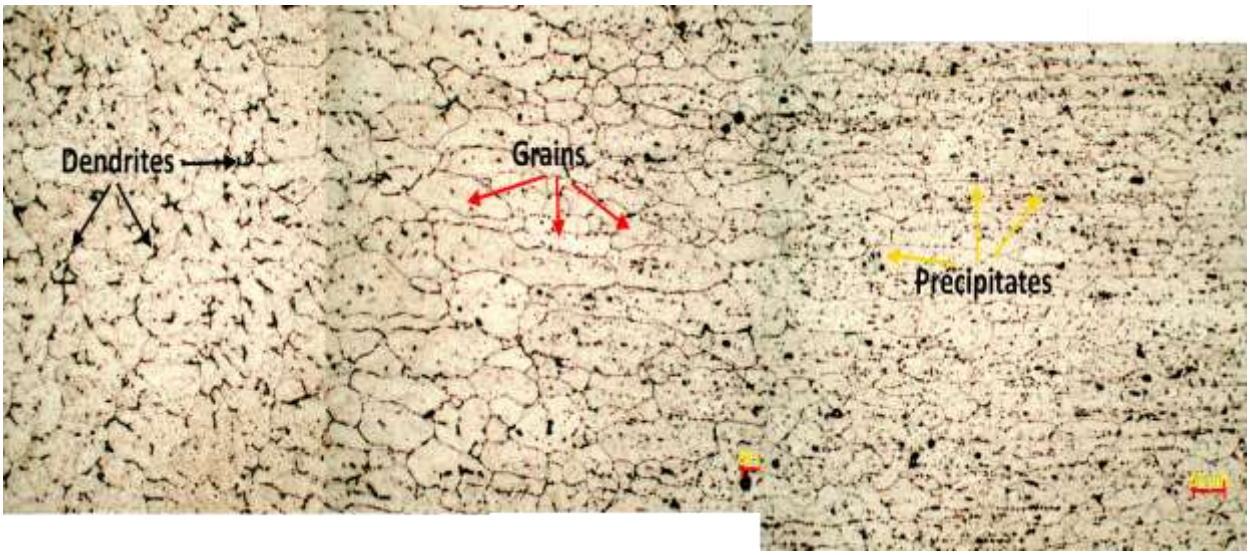

Figure 8. Microstructure at 200X of the HT sample. The micrograph shows Dendrites (black arrows) in the weld metal, elongated grains of Al (red arrows) in the HAZ, and coarse precipitates in the base metal (yellow arrows).

Figure 9 shows the microstructure in the HAZ, where EDS microanalysis was conducted. The results indicated that the precipitates were composed of Al, Fe, Si, and Mg. This finding is in agreement with published reports on Mg_2Si and FeSiAl precipitates in AA6061-T6[5–7], reinforcing the consistency of the microstructure with documented cases.

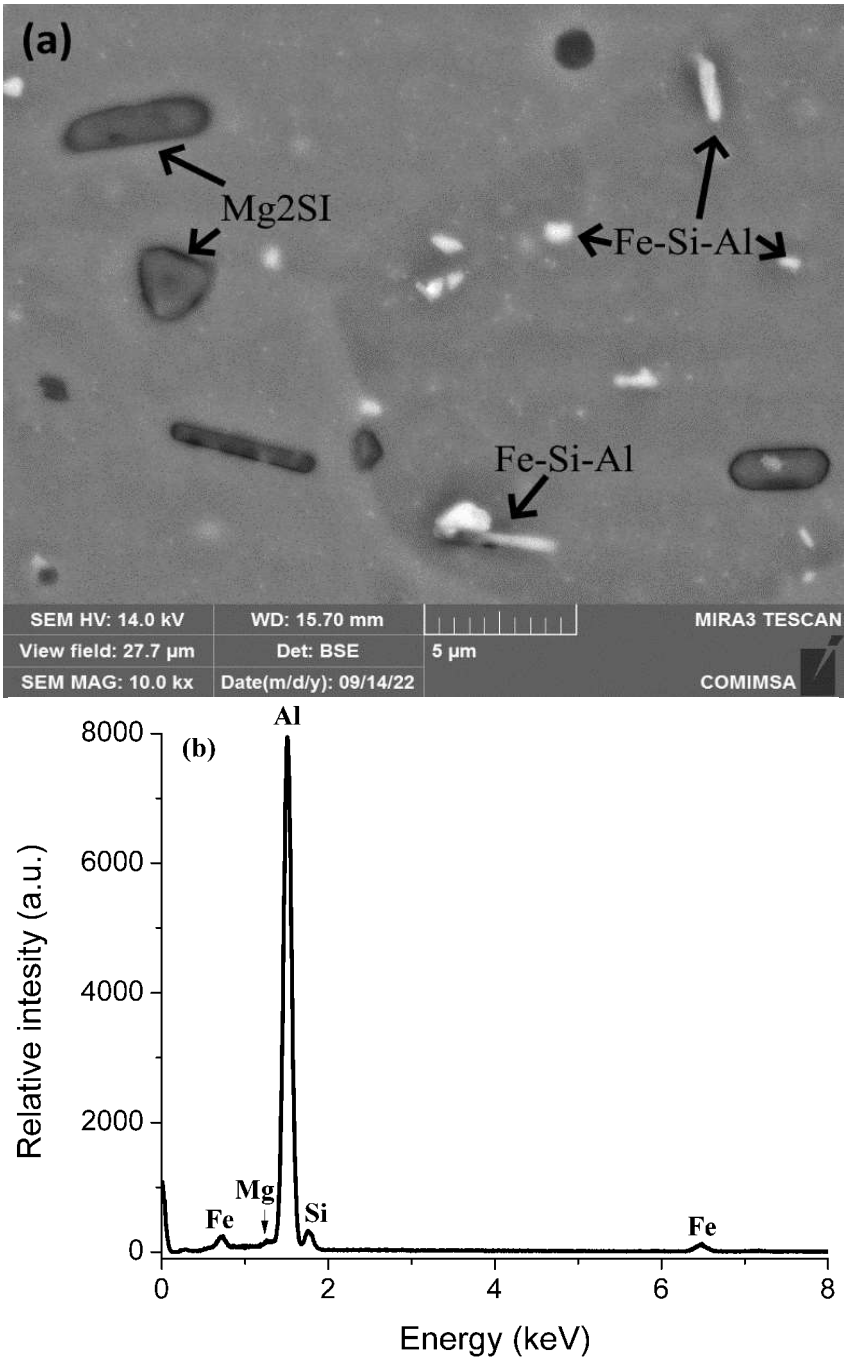

Figure 9. (a) SEM image using retro dispersive electrons shows precipitates in the base metal. (b) EDS pattern presents the microanalysis results exhibiting the precursor elements (Al, Fe, Si, Mg).

3.3 Fractographic observations

Fractographic examinations were conducted on the fracture surfaces of one specimen from each condition after tensile testing. The results consistently revealed a fracture pattern characterized by equiaxial dimples at the center of the specimens and shear dimples at the edges (Figures 10 a-d). These observations indicated a ductile fracture in all specimens. The location of the crack after the tensile test concided with this pattern, occurring at the end of the HAZ.

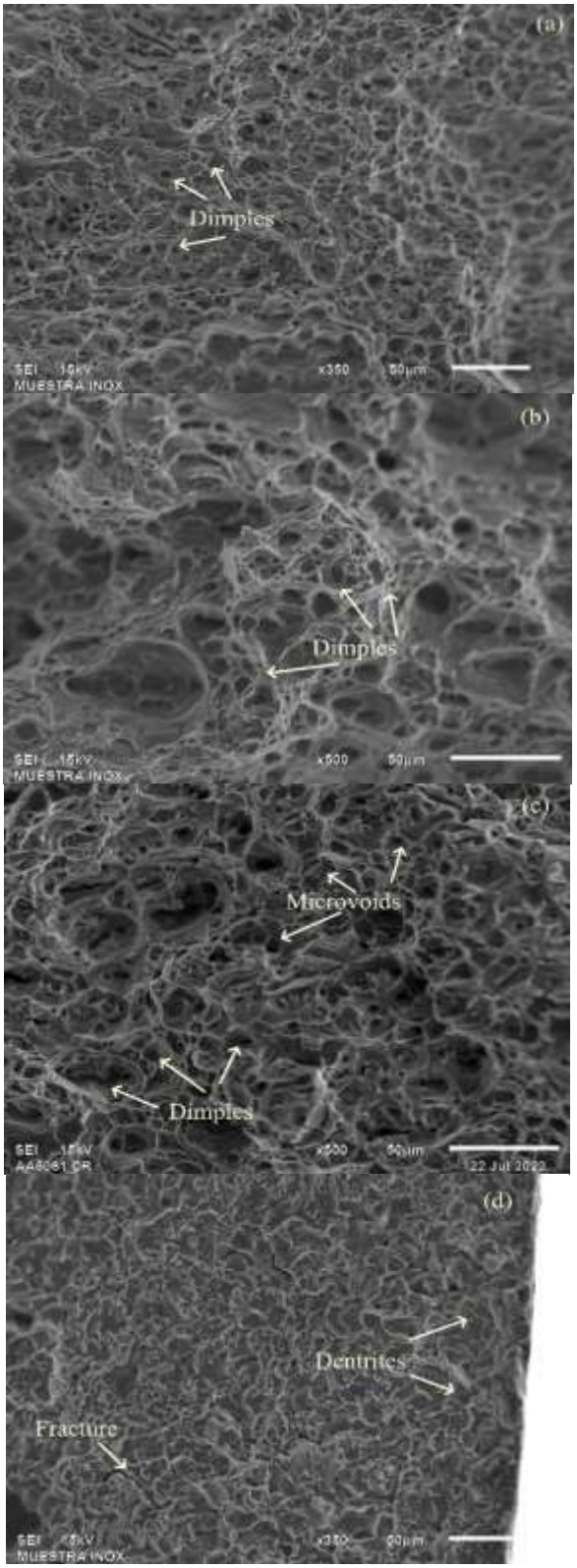

Figure 10. Examples of the fracture patterns of the room temperature tensile tested samples: (a) base metal, (b) "As welded" sample, (c) CT sample, and (d) HT sample.

However, the fractographic analysis of the heat-treated (HT) samples, as shown in Figure 10(d), demonstrated evidence of dimples, dendrites, and scattered porosity, particularly in the weld metal. This indicated the specific location of the crack in the HT sample within the weld metal.

Figure 11 presents the fracture pattern of the cryogenically treated (CR) sample at a high temperature (Ht, 90 °C), revealing a lack of fusion and tensile dimples. While the dimples suggested a ductile fracture in tensile mode, the lack of fusion is a welding defect with a significant impact on the mechanical properties. These fractographic features corresponded with the location of the crack reported in Table 1.

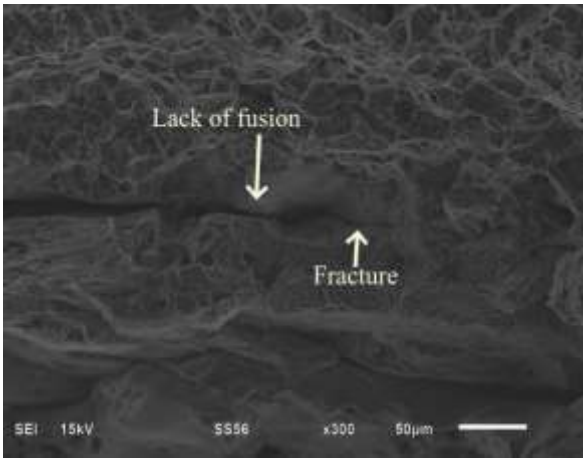

Figure 11. The fracture pattern of the tensile tested CR—Ht sample that failed in the weld metal. The fracture surface has dimples and no fusion.

Furthermore, the cracks were consistently located in the HAZ in the case of as-welded (AW) and cryogenically treated (CR) specimens. In contrast, for the heat-treated (HT) samples, cracks were identified in the weld metal, specifically in areas where welding defects such as pores were observed. This observation underscores the significant influence of post-welding heat treatment and welding defects on the mechanical properties of the specimens.

The evidence supporting this assertion is reinforced by instances where some AW and CR samples, exhibiting a visible lack of fusion, experienced cracking in the weld metal. Figures 10(a), 10(b) and 11 show several examples of the fracture patterns of these samples. These images illustrate the relationship between welding defects, heat treatment, and the resultant mechanical behavior.

Finally, Figure 12 displays the fracture pattern of the heat-treated (HT) sample at low temperature (Lt, -20 °C), exhibiting a lack of fusion and tensile dimples. Once again, these findings correlate with the location of the crack reported in Table 1.

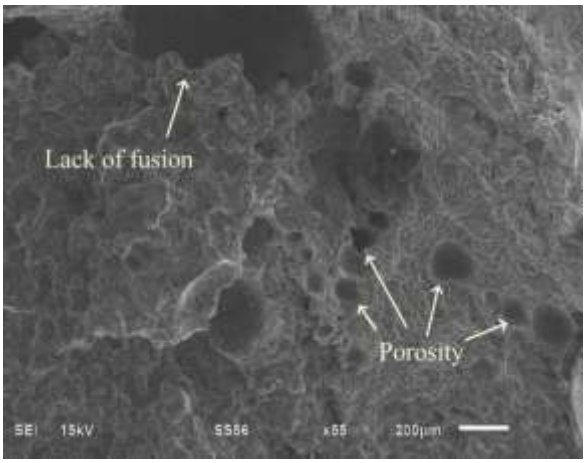

Figure 12. Fracture patterns of HT – Lt tensile sample that failed in the weld metal. There are dimples, alienated porosity, and a lack of fusion.

4. Discussion

Mechanical testing results for the 6061-T6 aluminum alloy indicated that all specimens met the minimum tensile strength requirements of AWS D1.23 except for the Rt-CR test specimens. Notably, the AW and HT test samples exhibited lower variability in tensile and yield strength across the test temperature range. In contrast, the CR test samples displayed a pronounced trend with temperature, showing a higher strength at low temperatures and a decrease as temperature increased[14,15]. This trend, however, was not consistently observed in other test results, except for the Ht (90 °C) specimens, where a decline in properties was noted. The reduction in the tensile strength for this specific condition was attributed to the presence of Al-Fe-Si precipitates in the microstructure, welding defects (mainly porosity and lack of fusion), and the FCC nature of aluminum alloys, which do not exhibit the ductile-to-brittle transition observed in BCC alloys such as steel[16].

The mechanical property variations were found to be dependent on the homogeneity of the test material, the sampling scheme, and other sources of variation[17]. The extensive microstructural changes induced by welding, coupled with welding defects like porosity or lack of fusion, significantly impacted the homogeneity of microstructural, micro, and macro mechanical properties[18,19].

The Vickers hardness testing revealed similar results for AW and CR test samples, with a more significant spreading in their weld metal and HAZ zone values compared to AW test results (see Figure 2). In contrast, the HT test specimens exhibited lower values in the weld metal (an average of 70 HV), while the values in the base metal and HAZ were close to those obtained in the base metal before welding (a mean of 100 HV).

As inferred from the mechanical testing results, joint efficiency depended on welding parameters, welding defects, and post-weld treatment[7,20]. Metallurgical changes induced by heat distribution during welding, welding-induced distortion, and residual stresses were identified as influencing factors, emphasizing the importance of post-weld heat treatment to mitigate these effects[21,22].

The observation of the base metal's macrostructure (see Figure 4) revealed a banded material with elongated grains of Al solid solution and precipitates with no

identified defects (i.e., cracks, incomplete or excessive fusion, cavities, etc.). The precipitates are constituted of Mg_2Si and Al-Fe-Si, consistent with the macroscopic results for the studied alloy[23].

The HAZ lengths for AW and CR test specimens were determined to be about 2.2 mm and 2.4 mm in length, respectively, while the HAZ for HT test specimens could not be identified, possibly due to the solution treatment. Lack of evidence for lack of fusion or incomplete penetration in macrographs was crucial, as these defects strongly influence weldment reliability and failure mode[24].

Microstructures of the weld metal were similar in the three welded samples, with the applied heat treatments showing limited impact on the morphology and size of dendrites because they are related to the cooling rate and solidification, as informed by Peng et al.[25]. Post-weld heat treatment effects were more pronounced in the HAZ microstructure. Overaging of the HAZ was identified as a factor reducing tensile strength and hardness in the weld[26,27]. The microhardness profiles illustrated this overaging effect, particularly in the HAZ induced by the weld thermal cycle[28].

AW test samples exhibited coarsening of precipitates in the HAZ, especially at grain boundaries, leading to reduced hardness in reference to the base metal, whose hardness has been reported up to 100 HV for AA6060-T6 alloy[28]. This reduction extended beyond the HAZ, emphasizing the influence of welding thermal cycles on microhardness. Due to aluminum's high thermal conductivity, thermal cycles are observed near the joint, propagating from the weld zone towards the base metal during the welding and in the opposite direction during cooling. These thermal cycles are caused by heat transfer, which occurs due to the energy input during the welding process. Once the heat input has stopped, the solidification begins from the base metal (the cooler region) towards the center of the weld pool (the hotter region). Then, during cooling, the heat transfer occurs in the reverse direction (from the weld to the base metal), generating different thermal gradients. The proximity to the weld zone determines the heat intensity, potentially leading to the formation of various phases between these regions. In this way, it has been indicated that the size and distribution of Mg_2Si phases affect the mechanical properties[29]. In our experimental results, as shown in Figure 9, a heterogeneous size distribution was obtained due to the changes in morphology, with an average size of 3.5 μm.

CR test samples showed stronger coarsening of precipitates, particularly in the HAZ, impacting hardness. However, a slight increase in hardness in the base metal suggested that overaging treatment induced coarsening of precipitates, which was more pronounced in the HAZ. Such coarsening has been found to strongly influence the hardness in the HAZ[23–29].

Microstructure analysis of HT test samples indicated effective precipitate dissolution through solution treatment while aging treatment restored mechanical properties. Microhardness profiles in the base metal aligned with literature values for AA6061-T6. The location of cracks after tensile testing in HT samples confirmed the effectiveness of the applied treatments.

Fractographic analysis revealed ductile fracture patterns in base metal, AW, and CR test samples, characterized by dimples in the center and shearing dimples at the edges. Lack of embrittlement due to precipitates at grain boundaries was indicated. In contrast, HT test samples exhibited a mix of tensile dimples, porosity, and dendrites, consistent with the location of cracks in the weld metal. The

influence of welding defects, particularly lack of fusion, on mechanical properties and crack place in AA6061-T6 weldments was underscored by fractographic evidence[30].

The fracture pattern in the HT test samples showed a mix of tensile dimples, porosity, and dendrites. This fracture pattern indicated a ductile fracture, which is explained by the location of the crack at the weld metal. Again, this evidence matched with the microstructure of the weld metal.

The heat treatment did not strongly modify the microstructure of the weld metal then it is feasible to say that some typical defects of the aluminum weld metal, such as pores and micro-cracks, remained in the microstructure of such area and played a role in the crack growth during the tensile test. This fact has already been explained in technical literature[30–32].

5. Conclusions

This study explored the mechanical and microstructural behavior of Gas Tungsten Arc Welding (GTAW) butt-welded 6061-T6 Aluminum alloy subjected to various heat treatment conditions after the welding process and tensile testing temperatures. Several key conclusions emerged from this research:

1. Temperature-dependent mechanical properties: The mechanical testing results demonstrated a temperature-dependent behavior, with the as-welded (AW) and heat-treated (HT) specimens exhibiting lower variability in tensile and yield strength across different temperatures. Cryogenic treatment (CR) revealed a distinct trend, exhibiting higher tensile strength at low temperatures and a subsequent decrease as the temperature rises.

2. Influence of post-weld heat treatment: Post-weld heat treatments (HT) restore mechanical properties, effectively dissolving precipitates through a solutionizing treatment and contributing to overall joint efficiency. Also, microhardness profiles show the impact of heat treatments on the hardness distribution, with HT samples exhibiting higher values in the HAZ and base metal.

3. Microstructural transformations: Microstructural analyses revealed the persistence of dendritic structures in weld metal across different conditions, highlighting the limited influence of applied heat treatments on their morphology. Overaging effects were observed in CR samples, particularly in the HAZ, whereas HT samples demonstrated effective dissolution of precipitates in the base metal.

4. Fractographic evaluation: Fractographic examinations exhibited the fracture patterns, showing ductile characteristics in base metal, AW, and CR samples, with evidence of dimples indicative of ductile fracture. HT samples displayed a distinct fracture pattern characterized by a mix of tensile dimples, porosity, and dendrites, aligning with the location of cracks in the weld metal. Lack of fusion is a significant factor influencing mechanical properties and crack location.

These findings suggest practical implications for improving welding processes and heat treatments to enhance the reliability and performance of aluminum alloy weldments. Future research may explore other relationships between welding parameters, post-weld treatments, and microstructural changes, considering additional factors such as welding speed and thermal efficiency.

References

1. Georgantzia, E., Gkantou, M. & Kamaris, G. S. “Aluminium alloys as structural material: A review of research”. *Eng.*

Struct. 227, 111372 (2021). 10.1016/j.engstruct.2020.111372.

2. Materials and applications, Part 1. in *Welding handbook* (eds. Connor, L. P., O'Brien, R. L., Oates, W. R. & American Welding Society) vol. Volume 3 (American Welding Society, 1987).

3. *AWS D1.2/D1.2M Structural Welding Code - Aluminum*. 83–87 (2013).

4. Habibi, I., Triyono & Muhayat, N. A "Review on Aluminum Arc Welding and It's Problems". in *Proceedings of the 6th International Conference and Exhibition on Sustainable Energy and Advanced Materials* (eds. Sabino, U., Imaduddin, F. & Prabowo, A. R.) 819–826 (Springer Singapore, 2020). 10.1007/978-981-15-4481-1_78.

5. Ramaswamy, A., Malarvizhi, S. & Balasubramanian, V. "Post-weld heat treatment effects on the tensile properties of cold metal arc welded AA 6061-T6 aluminum joints". *Mater. Test.* 62, 69–76 (2020). 10.3139/120.111454

6. Rathinasuriyan, C., Kumar, V. S. S. & V, S. "Mechanical and Metallurgical Properties of GTAW, GMAW and FSW Lap Joints on AA6061-T6 Alloy". *Adv. Mater. Process. Technol.* 8, 3231–3247 (2022). 10.1080/2374068X.2021.1946322

7. Guzmán, I. *et al.* "Tensile and fracture behavior in 6061-T6 and 6061-T4 aluminum alloys welded by pulsed metal transfer GMAW". *Int. J. Adv. Manuf. Technol.* 103, 2553–2562 (2019). 10.1007/s00170-019-03673-7

8. Rodríguez-Hernández, T. *et al.* "First assessment on the microstructure and mechanical properties of gtaw-gmaw hybrid welding of 6061-t6 AA". *J. Manuf. Process.* 59, 658–667 (2020). 10.1016/j.jmapro.2020.09.069

9. Soundararajan, R., Ramkumar, K. R., Sivasankaran, S. & Kim, H. S. "Enhancement of tensile strength in AA 6061-T6 plates joined by gas tungsten arc welding using high entropy alloy filler sheet". *Mater. Sci. Eng. A* 832, 142481 (2022). 10.1016/j.msea.2021.142481

10. Anderston, T. *Welding aluminum: questions and answers: a practical guide for troubleshooting aluminum welding-related problems*. (American Welding Society, 2010).

11. ASTM International. ASTM E8/E8M - 16a Standard Test Methods for Tension Testing of Metallic Materials. in *ASTM Volume 03.01 Metals – Mechanical Testing; Elevated and Low-Temperature Tests; Metallography* vol. 03.01 (ASTM International, 2016).

12. ASTM International. ASTM E3-11 (2017) Standard Guide for Preparation of Metallographic Specimens. in *ASTM Volume 03.01 Metals – Mechanical Testing; Elevated and Low-Temperature Tests; Metallography* vol. 03.01 (ASTM International, 2017).

13. Dowling, N. E. & App, B. "Statistical variation in materials properties". in *Mechanical Behavior of Materials* 798–806 (Prentice-Hall).

14. Matweb. Material Property Data Aluminum 6061-T6. https://asm.matweb.com/search/specificmaterial.asp?bassnum=ma6061t6. Retrieved November 20th, 2023.

15. The American Society of Mechanical Engineers. *BPVC Section II-Materials-Part D-Properties-(Customary)*. (ASME, 2023).

16. Askeland, D. R. *The Science and Engineering of Materials*. (Springer US: Imprint: Springer, 1996).

17. Pan, M. *et al.* "A Study on Welding Characteristics, Mechanical Properties, and Penetration Depth of T-Joint Thin-Walled Parts for Different TIG Welding Currents: FE Simulation and Experimental Analysis". *Metals* 12, 1157 (2022). 10.3390/met12071157

18. Evdokimov, A., Obrosov, A., Ossenbrink, R., Weiß, S. & Michailov, V. "Mechanical properties of dissimilar steel-aluminum welds". *Mater. Sci. Eng. A* 722, 242–254 (2018). 10.1016/j.msea.2018.03.019

19. Samiuddin, M. *et al.* "Investigation on the process parameters of TIG-welded aluminum alloy through mechanical and microstructural characterization". *Def. Technol.* 17, 1234–1248 (2021). 10.1016/j.dt.2020.06.012

20. Gómora, C. M., Ambriz, R. R., Curiel, F. F. & Jaramillo, D. "Heat distribution in welds of a 6061-T6 aluminum alloy obtained by modified indirect electric arc". *J. Mater. Process. Technol.* 243, 433–441 (2017). 10.1016/j.jmatprotec.2017.01.003

21. Park, K. *et al.* "Effects of Cryogenic Treatment on Residual Stress and Tensile Properties for 6061 Al Alloy". *Taehan-Kŭmsok-Hakhoe-Chi J. Korean Inst. Met. Mater.* 49, 9–19 (2011).

22. Lakshminarayanan, A. K., Balasubramanian, V. & Elangovan, K. "Effect of welding processes on tensile properties of AA6061 aluminium alloy joints". *Int. J. Adv. Manuf. Technol.* 40, 286–296 (2009). 10.1007/s00170-007-1325-0

23. Ribeiro, A. S. & De Jesus, A. M. P. "Fatigue Behaviour of Welded Joints Made of 6061-T651 Aluminium Alloy". in *Aluminium Alloys, Theory and Applications* (ed. Kvackaj, T.) (InTech, 2011). doi:10.5772/14489.

24. Wang, B., Xue, S., Ma, C., Wang, J. & Lin, Z. "Effects of Porosity, Heat Input and Post-Weld Heat Treatment on the Microstructure and Mechanical Properties of TIG Welded Joints of AA6082-T6". *Metals* 7, 463 (2017). 10.3390/met7110463

25. Peng, D., Shen, J., Tang, Q., Wu, C. & Zhou, Y. "Effects of aging treatment and heat input on the microstructures and mechanical properties of TIG-welded 6061-T6 alloy joints". *Int. J. Miner. Metall. Mater.* 20, 259–265 (2013). 10.1007/s12613-013-0721-8

26. Wang, J., Chen, X., Yang, L. & Zhang, G. "Effect of preheat & post-weld heat treatment on the microstructure and mechanical properties of 6061-T6 aluminum alloy welded sheets". *Mater. Sci. Eng. A* 841, 143081 (2022). 10.1016/j.msea.2022.143081

27. Cheng, J. *et al.* "Improving heat-affected zone softening of aluminum alloys by in-situ cooling and post-weld rolling". *J. Mater. Process. Technol.* 306, 117639 (2022). 10.1016/j.jmatprotec.2022.117639.

28. Yi, J., Wang, G., Li, S., Liu, Z. & Gong, Y. "Effect of post-weld heat treatment on microstructure and mechanical properties of welded joints of 6061-T6 aluminum alloy". *Trans. Nonferrous Met. Soc. China* 29, 2035–2046 (2019). 10.1016/S1003-6326(19)65110-1

29. Dewan, M. W., Wahab, M. A. & Okeil, A. M. “Influence of Weld Defects and Postweld Heat Treatment of Gas Tungsten Arc-Welded AA-6061-T651 Aluminum Alloy”. *J. Manuf. Sci. Eng.* 137, 051027 (2015). 10.1115/1.4030333

30. Verma, R. P. & Kumar Lila, M. “A short review on aluminium alloys and welding in structural applications”. *Mater. Today Proc.* 46, 10687–10691 (2021). 10.1016/j.matpr.2021.01.447

31. Liu, F. J., Fu, L. & Chen, H. Y. “Microstructure evolution and fracture behaviour of friction stir welded 6061-T6 thin plate joints under high rotational speed”. *Sci. Technol. Weld. Join.* 23, 333–343 (2018). 10.1080/13621718.2017.1389837

32. Zhang, L. *et al.* Microstructure, mechanical properties and fatigue crack growth behavior of friction stir welded joint of 6061-T6 aluminum alloy. *Int. J. Fatigue* 135, 105556 (2020). 10.1016/j.ijfatigue.2020.105556